Int J Adv Manuf Technol (2017) 88:1141–1150
DOI 10.1007/s00170-016-8837-4

ORIGINAL ARTICLE

Elucidation of high-power disk laser welding phenomena by simultaneously observing both top and bottom of weldment

Ziqin Chen[1] · **Xiangdong Gao**[1] · **Seiji Katayama**[2] · **Zhenlin Xiao**[3] · **Xiaohui Chen**[3]

Received: 9 September 2015 / Accepted: 25 April 2016 / Published online: 6 May 2016
© Springer-Verlag London 2016

Abstract A method is introduced to investigate the interrelationships among welding penetration rate, spatter number, metallic vapor, and welding quality by simultaneously observing both top surface and bottom surface of low carbon steel weldment during high-power disk laser welding. Color image segmentation algorithm which is based on K-means clustering algorithm is used to process the image data. Different welding conditions including different weld power, weld speed and weld joint width are applied, and the microstructures of fusion part are also analyzed. Experiment results show that the color image segmentation algorithm is effectively for recognition of welding penetration condition, and welding quality is better when the penetration rate is around 74.5 %.

Keywords High-power laser welding · Full-penetration condition · Color image segmentation algorithm · Welding characteristic detection

✉ Xiangdong Gao
gaoxd666@126.com

[1] Guangdong Provincial Key Laboratory of Computer Integrated Manufacturing, School of Electromechanical Engineering, Guangdong University of Technology, No.100 West Waihuan Road, Higher Education Mega Center, Panyu District, Guangzhou 510006, China

[2] Joining and Welding Research Institute, Osaka University, 11-1 Mihogaoka, Ibaraki, Osaka 567-0047, Japan

[3] Guangzhou Panyu Gofront Dyeing & Finishing Machinery Manufacturer Co.,Ltd, Guangzhou 511400, China

1 Introduction

Laser welding is an effective and reliable method for material joint processing, due to its various advantages such as the concentrated heat power, small heat-affected zone, high-speed production and high-quality shaping, laser welding is largely applied in plenty of industrial productions [1–4]. Low-carbon steel is the most wildly used in many engineering machinery structures due to its desirable mechanical properties including good weld ability [5]. The various phenomena generated during laser welding have very close relationship with welding quality and stability, such as plume, spatter [6], and dynamic molten pool [7, 8]. There are lots of researches for detecting the welding quality through observing the various phenomena, which are captured mostly based on visual sensor, and analyzed by different on-line [9] or off-line image processing algorithm [10–13]. Moreover, all these phenomena are related to penetration condition, which is depended on the focal position while the welding condition is the same [14, 15]. When laser power is relatively lower, weld would be lack of penetration which may cause weld defeats such as porosities and cracks. And when laser power becomes higher, weld would be full penetration which is an ideal state of welding. And if laser power continues to become stronger, weld defeats such as excessive penetration, surface depression, cracks and even laser cutting would be generated [16, 17]. Therefore, penetration condition is an important characteristic for welding quality detection.

In order to figure out the relationship between welding quality and penetration condition, the situation of bottom surface should be observed directly. Multi kinds of visual sensor is wildly sued in various aspects as detection and monitoring, for its advantages such as non-contact, visualized, high-speed, and convenient to capture different kinds of images, like infrared image, ultraviolet image, radiographic image, magneto-

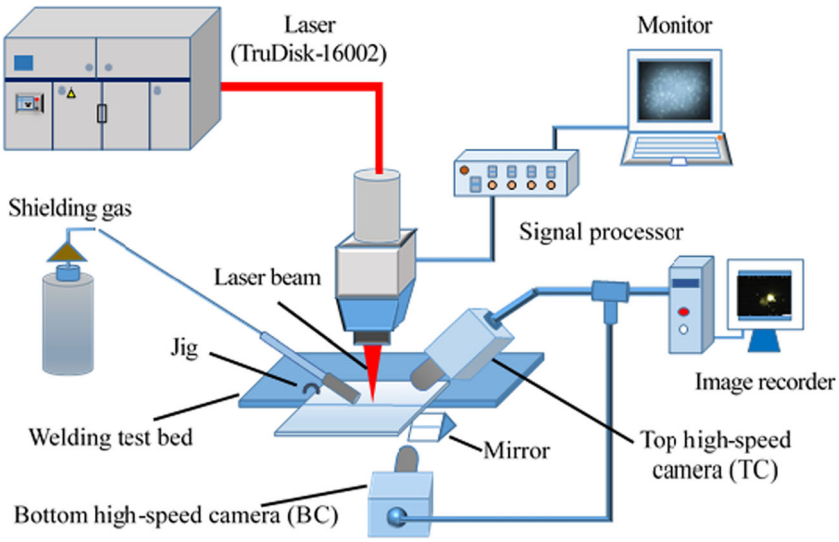

Fig. 1 Experimental setup of high-power disk laser welding

optical image, and visible image, which are containing lots of information of the observation objects [18–21]. And multi-sensor systems have been investigated in recent years for ensuring product quality [22]. In which color image contains more feature information of observed object as it could be segmented into multi-level images [23–25]. This paper presents an experimental system which has two high-speed cameras and could inspect both top surface and bottom surface of weldment during high-power disk laser welding process, and the one focus on bottom surface of weldment acquires visible images. Laser power, weld joint width, and weld speed are changed, and spatter, metallic vapor, and keyhole of bottom surface characteristics are calculated under these different welding conditions. The rules are summarized through color image segmentation algorithm, microstructures of weldment are also observed. The result shows the characteristics are closely related to welding quality.

2 Experimental setup

The experiment facility is shown as Fig. 1. It is performed with a high-power disk laser equipment TruDisk-16002, the maximum power of which is 16 kW, the laser wavelength is 1030 nm, and the laser beam diameter is 280 μm. Two high-speed cameras and a computer are used as imaging capture system. Top high-speed camera (TC) is in front of the weldment and perpendicular to the welding direction, infrared-visible optical filter is used to capture metallic vapor and spatter of weldment top surface. Bottom high-speed camera (BC) is placed beside the weldment and focuses on the laser focuses position, which is reflected by the mirror; visible optical filter is used to obtain the phenomena of weldment bottom surface. Metal active gas (MAG, which is combined by 80 % of Ar and 20 % of CO_2) is used as shielding gas, its flow is set as 30 L/min and the nozzle angle is 42°. Low-carbon steel SS400 is used as weldment and its components content are shown as Table 1. The size of one piece of weldment plate is 150 mm × 60 mm × 6 mm (length × width × thickness). In order to get full penetration, the focus of laser is set as −2 mm.

Welding conditions are changed in three aspects, weld joint width are set as 0, 0.05, and 0.1 mm, weld power are set as 3 and 4 kW, weld speed are set as 1, 1.5, and 2 m/min. Fifteen groups of experiments are performed in total. Details of each welding condition are denoted by Table 2, in

Table 1 Chemical composition of low-carbon steel SS400

Material	C	Mn	P	S
SS400	–	–	≤0.05 %	≤0.05 %

Table 2 Details of each welding condition

D/mm	0					0.05					0.1				
P/kW	4			3		4			3		4			3	
V/(m/min)	1	1.5	2	1	1.5	1	1.5	2	1	1.5	1	1.5	2	1	1.5
No.	a	b	c	d	e	f	g	h	i	j	k	l	m	n	o

which D represents width of weld joint, P represents laser power, V represents weld speed and No. is sequence of the image data.

The top view and bottom view of all the welded weldments are shown as left column of Fig. 2, and one of their relevant top surface condition and bottom surface condition images at

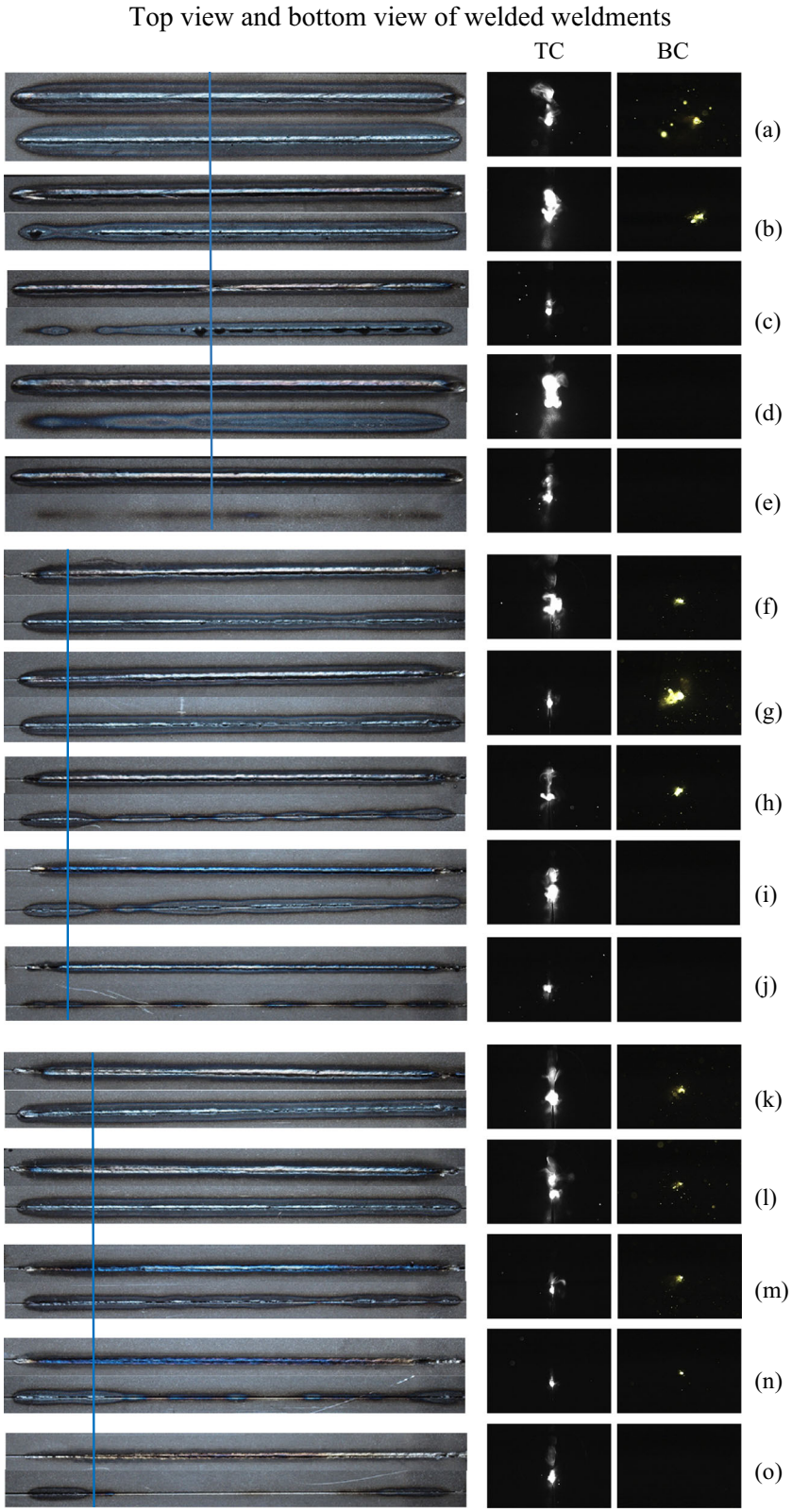

Fig. 2 Top view and bottom view of weldments and their relevant images

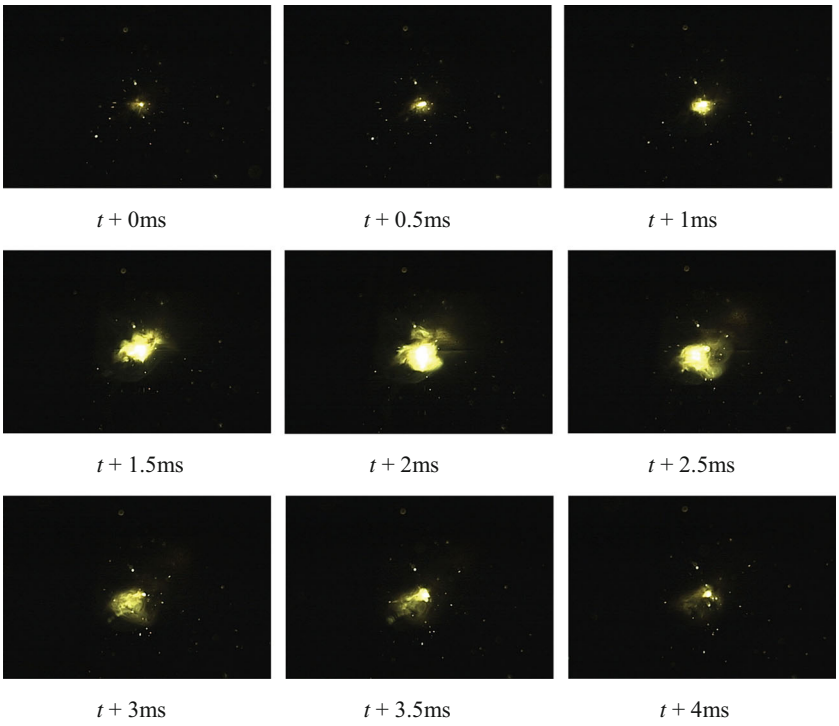

Fig. 3 Sequence images of bottom view during high-power laser welding

the indicated position, obtained by top high-speed camera and bottom high-speed camera during high-power laser welding, are shown as TC and BC in Fig. 2.

3 Characteristic information extraction of welding data

3.1 Principle of color image segmentation algorithm

The image data recorded by the high-speed camera which is focused on the bottom surface are colorized, then the main characteristic information of laser welding could be observed. A sequence of bottom surface image is shown as Fig. 3.

Because the visual sensor of bottom surface is colorized, then a color image segmentation algorithm is used to process the images. The principle of color image segmentation algorithm is that the RGB image could be transform into other color spaces, and single-dimensional histogram of each space could be work out, then the most significant peak value would be selected as threshold [21]. Clustering algorithm is a self-trained classifier, which means it can perform image classification and extract various types of characteristic value

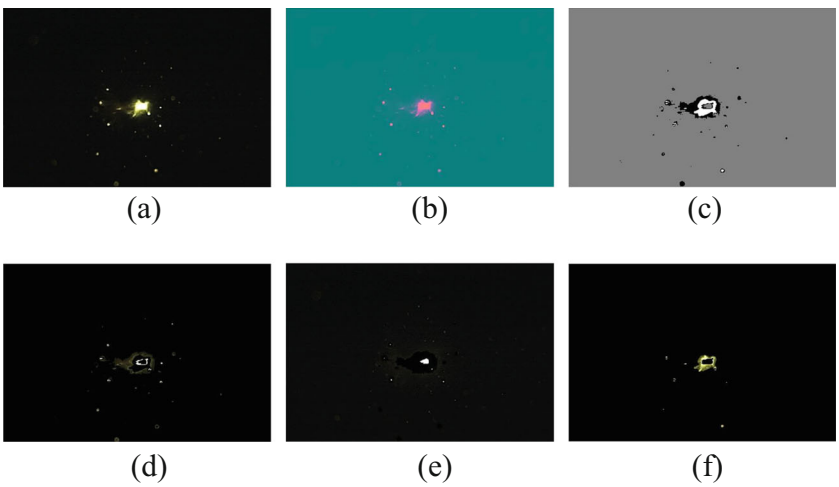

Fig. 4 Image process, **a** is original RGB image of bottom surface, **b** is $L \times a \times b$ color space image, **c** is pixels marked image by K means clustering algorithm, **d** is "L" layer image, **e** is "a" layer image, and **f** is "b" layer image

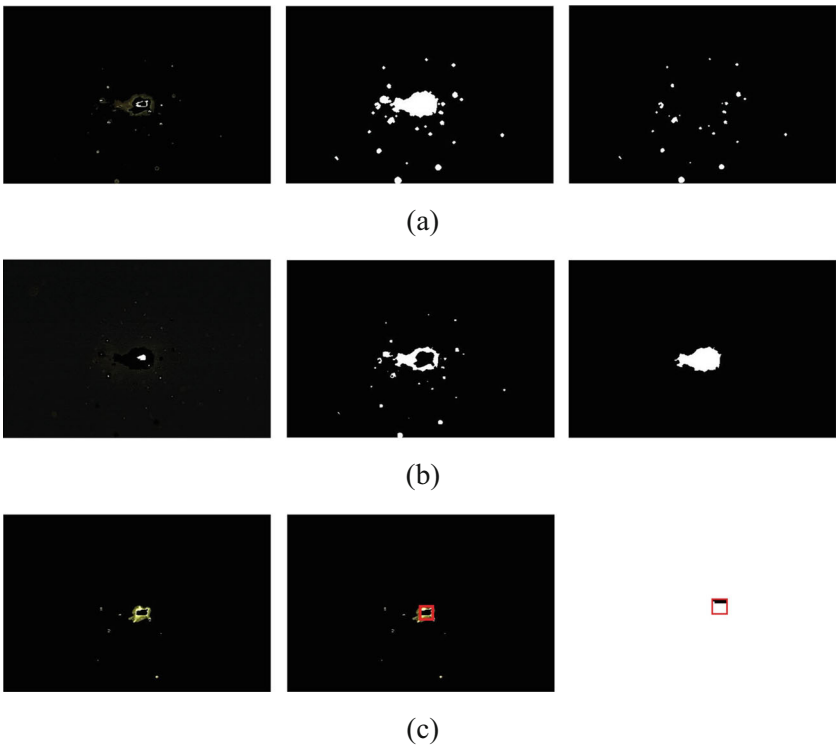

Fig. 5 Capture of characteristics, **a** is capture of spatter, **b** is capture of metallic vapor, **c** is judgment of full-penetration condition

iteratively. Fuzzy K-means clustering algorithm is an unsupervised statistical algorithm and it does not need training sample.

First step of fuzzy K-means clustering algorithm is to average each of current categories, and then follow the mean value of the new generation to reclassify the pixels, the pixels will be classified into the most recent category. The details of process is shown as follow.

Step 1. Take any K attribute values ($Y_1(n)$, $Y_2(n)$, …, $Y_l(n)$, $Y_k(n)$) as the centers of the initial groups. Set cycle number as N and set its initial value as 1.

Step 2. X represents all property value vectors and it is classified as formula (1), in order to make vector value of vector set $\{X\}$ belongs to $S_1(n)$, $S_2(n)$, …, $S_l(n)$, $S_k(n)$, which are corresponding subsets of $Y_1(n)$, $Y_2(n)$, …, $Y_l(n)$, $Y_k(n)$.

$$d_l = \min\{d_j\} \rightarrow X \in S_l(n), N \equiv \{1, 2, \ldots, K\} \quad (1)$$

Step 3. d_j is the distance between X and $Y_j(n)$, defined as follow:

$$d_j \equiv \left\| \mathrm{X} - \mathrm{Y_j}(n) \right\| \quad (2)$$

Step 4. New center $Y_l(n+1)$ of each subset $S_l(n)(l = \{1,2,3, \ldots,K\})$ is calculated as follow:

$$Y_l(n+1) = \frac{1}{N_l} \sum\nolimits_{X \in S_L(n)} X \quad (3)$$

in which, N_l is element number of set $S_l(n)$.

Step 5. The circular process is over when the formula below is tenable for all groups,

$$Y_l(n+1) = Y_l(n), l \in N_K \quad (4)$$

Otherwise, return to step 2 to continue processing.

3.2 Image data processing

K means clustering algorithm is used for image segmentation based on the color space. A color image of bottom surface is taken as example shown as Fig. 4. The color space of the image is changed from RGB color space into $L \times a \times b$ color space. Then K means clustering algorithm is used to classify the color of $L \times a \times b$

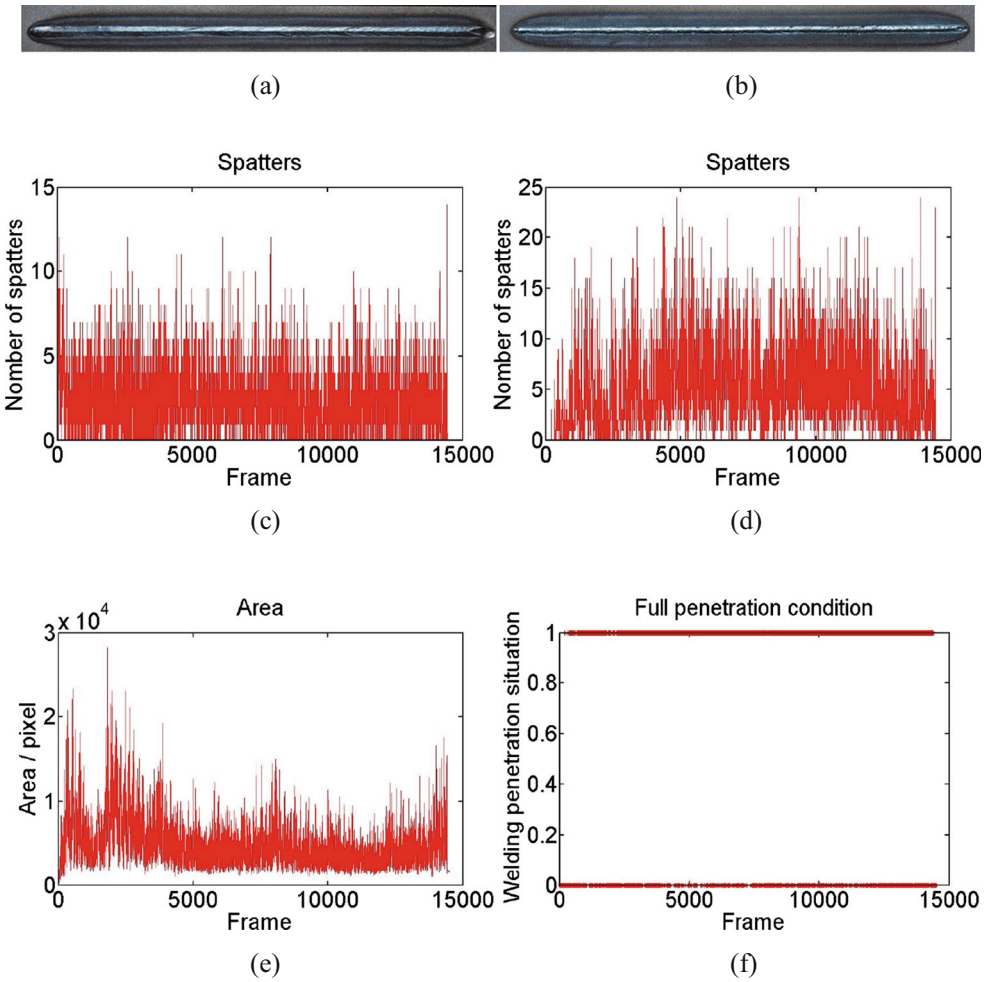

Fig. 6 Characteristics aggregate of weldment a, in which **a** is top view, **b** is bottom view, **c** and **d** are spatter number captured by top and bottom high-speed cameras respectively, **e** is metallic vapor area captured by top high-speed camera, **f** is judgment of penetration condition captured by bottom high-speed camera

color space, and mark the pixels of image according to the classified result.

The "*L*" layer image is selected to calculate the number of spatter, "*a*" layer image is used to detect the metallic vapor, and "*b*" layer image is served as judgment for full-penetration condition. As "*L*" layer represents luminance, spatial filter processing is used to remove noise, image enhancement processing is used to enhance contrast, then metallic vapor section is subtracted, and the number of spatters could be calculated. And morphological image processing and spatial filter processing are also used to capture the metallic vapor characteristics of "*a*" layer. Because the location of keyhole is fixed, then the section of keyhole is selected as object. Color image segmentation processing is used to mark and segment the keyhole section of "*b*" layer, and after image processing, if the number of marked pixels (which are equal to 1) of the selected section, is greater than a constant, it would be judged as full penetration. The brief processing procedures are shown as Fig. 5. Detection of spatter, metallic vapor and full-penetration condition are shown as Fig. 5a, b, c, respectively. As Fig. 5c shows, the amount of pixel which is 1, is more than half of the amount of all pixels of the selected section after image processing, then the condition at this moment is judged as full penetration.

The characteristics detection of weldment a are shown as Fig. 6. In which, panel a is top view of weldment a, panels c and e are the statistical analyses of spatter number and metallic vapor area, which are captured by top high-speed camera of weldment a. Panel b is bottom view of weldment a, panels d and f are statistical analyses of spatter number and judgment of full-penetration condition, which are captured by bottom high-speed camera of weldment a.

The characteristics detection of weldment b are shown as Fig. 7. And panel a is top view of weldment

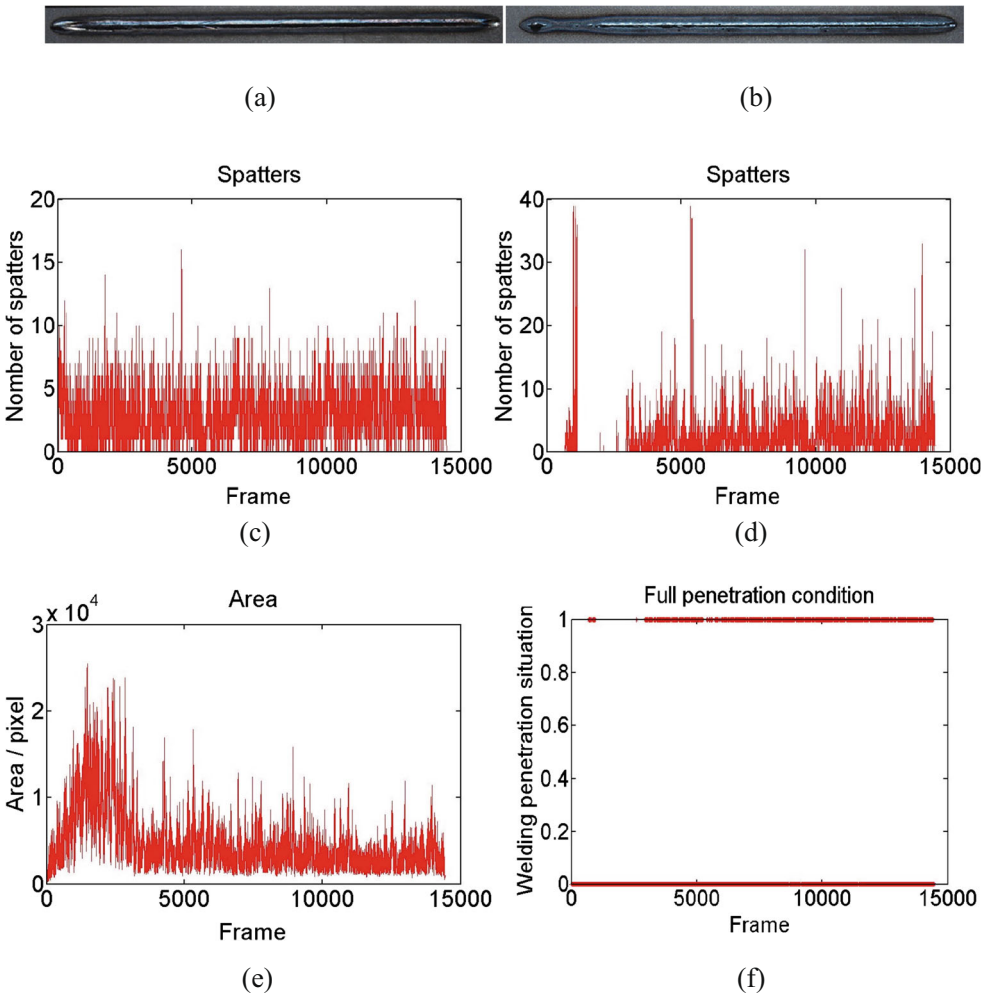

Fig. 7 Characteristics aggregate of weldment b, in which **a** is top view, **b** is bottom view, **c** and **d** are spatter number captured by top and bottom high-speed cameras respectively, **e** is metallic vapor area captured by top high-speed camera, **f** is judgment of penetration condition captured by bottom high-speed camera

b, panels c and e are statistical analyses of spatter number and metallic vapor area, which are captured by top high-speed camera of weldment b. Panel b is bottom view of weldment b, Panels d and f are statistical analyses of spatter number and judgment of full-penetration condition, which are captured by bottom high-speed camera of weldment b. All these characteristics have obvious fluctuation along with welding forming and welding quality.

4 Analysis of welding results

In order to investigate the relationship between the full-penetration condition and welding quality, the macro-structure of weldments' transverse section are shown as lift of Fig. 8, and penetration condition judged by proposed color image segmentation algorithm based on K-means clustering algorithm, are shown as right of Fig. 7, in which full-penetration condition is represented by 1, and incompletely penetration condition is represented by 0.

By comparing panels a and b of Fig. 8, it is obvious that more weld defects like weld porosities are prone to arise while the welding penetration is incompletely, and these pores may cause serious damages, which is not good for welding quality. In comparison of real macro-structure and penetration condition, which is worked out by proposed color image segmentation algorithm, shows that this algorithm is credible for judgment of full-penetration condition, and could offer a theoretical foundation for welding quality monitoring.

Microstructures of fusion section are shown in Fig. 9, in which A is fusion zone, B is heat-affected zone and C is base material. Relationships between weld joint width, welding speed, laser power, spatter number, and

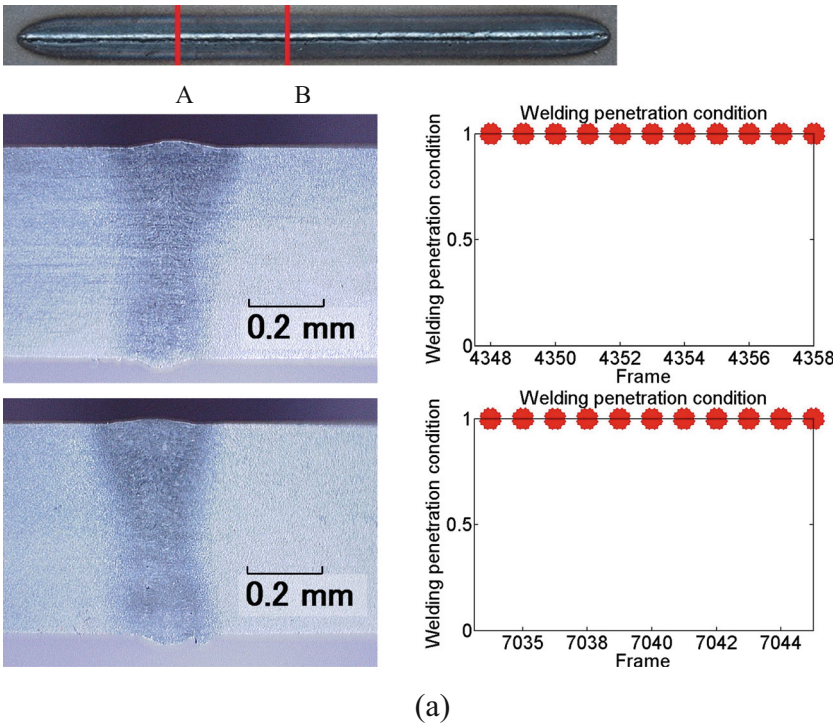

(a)

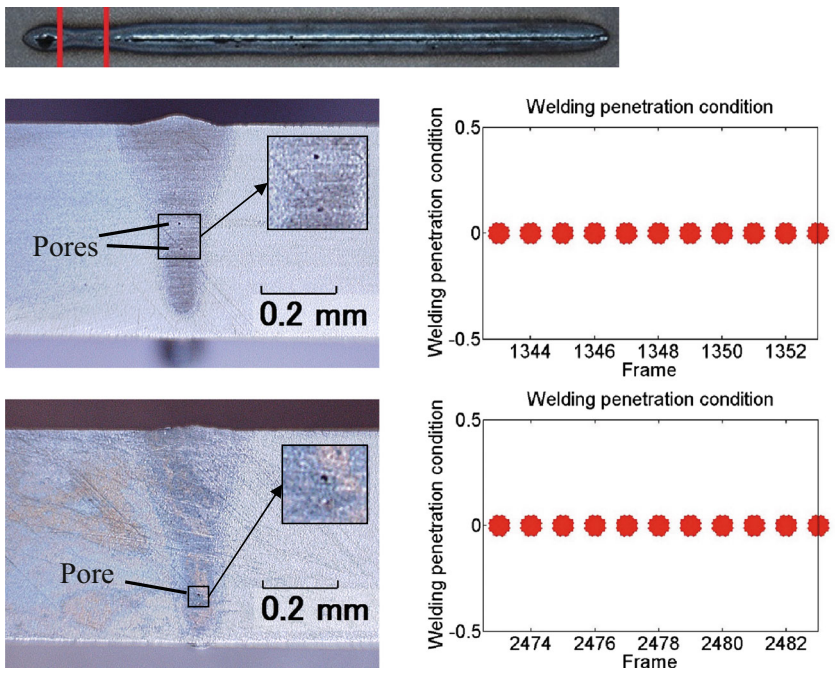

(b)

Fig. 8 Macrostructure of weldments' transverse section, **a** is macrostructure and penetration condition judgment of weldment a, **b** is macrostructure and penetration condition judgment of weldment b

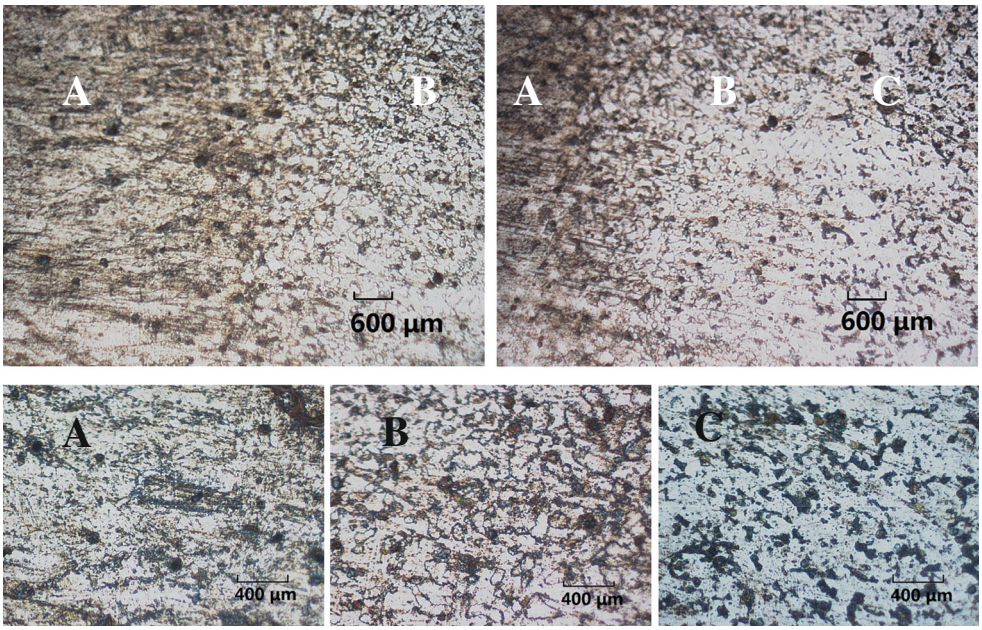

Fig. 9 Microstructures of weld transverse section obtained by optical microscope

penetration condition of bottom surface are shown as Fig. 10.

5 Conclusion

Compared with macrostructure of weldment transverse section, the proposed color image segmentation algorithm based on K-means clustering algorithm is credible for detecting characteristics through image data captured by high-speed cameras, and this could provide a theoretical guidance for welding quality automatic control.

Rules for high-power laser welding of low-carbon steel SS400 which thickness is 6 mm are summarized as follows. (1) Tendency of penetration rate and spatter number are consistent. (2) Penetration rate and spatter number are fluctuating decreasing as the weld speed increasing. (3) Penetration rate and spatter number are sharply decreasing as laser power decreasing. (4) Penetration rate and spatter number are increasing as weld joint width

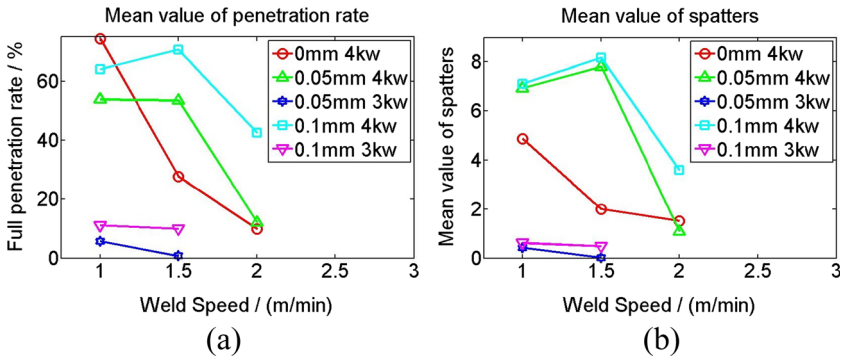

Fig. 10 Relationships between characteristics of bottom surface, **a** is mean value of penetration rate of 13 groups, **b** is mean value of spatter number of 13 groups

increasing. (5) Under this welding condition, the best full penetration rate is around 74.5 %, which could obtain a sound welding quality.

Acknowledgments This work was partly supported by the National Natural Science Foundation of China (grant no. 51175095), the Science and Technology Planning Project of Guangzhou, China (grant no. 201510010089), the Science and Technology Planning Major Project of Guangdong Province, China (grant no. 2014B090921008), the Coordination Innovation and Platform Environment Construction Project of Guangdong Province, China (grant no. 503149102077), and the Science and Technology Planning Public Project of Guangdong Province, China (Grant No. 509197855073).

References

1. You DY, Gao XD, Katayama S (2014) Monitoring of high-power laser welding using high-speed photographing and image processing. Mech Syst Signal Process 49:39–52
2. Meng W, Li ZG, Huang J, Wu YX, Katayama S (2014) Microstructure and softening of laser-welded 960 MPa grade high strength steel joints. J Mater Eng Perform 23:538–544
3. You DY, Gao XD, Katayama S (2013) Multiple-optics sensing of high-brightness disk laser welding process. NDT&E Int 60:32–39
4. You DY, Gao XD, Katayama S (2014) Review of laser welding monitoring. Sci Technol Weld Join 19:181–201
5. Benasciutti D, Lanzutti A, Rupil G, Haeberle FE (2014) Microstructural and mechanical characterisation of laser-welded lap joints with linear and circular beads in thin low carbon steel sheets. Mater Des 62:205–216
6. Gao XD, Wen Q, Katayama S (2013) Analysis of high-power disk laser welding stability based on classification of plume and spatter characteristics. Trans Nonferrous Metals Soc China 23:3748–3757
7. Li SC, Chen GY, Katayama S, Zhang L (2014) Relationship between spatter formation and dynamic molten pool during high-power deep-penetration laser welding. Appl Surf Sci 303:481–488
8. You DY, Gao XD, Katayama S (2014) Visual-based spatter detection during high-power disk laser welding. Opt Lasers Eng 54:1–7
9. Ruisz J, Biber J, Loipetsberger M (2007) Quality evaluation in resistance spot welding by analyzing the weld fingerprint on metal bands by computer vision. Int J Adv Manuf Technol 33:952–960
10. Chen HC, Bi GJ, Nai MLS, Wei J (2015) Enhanced welding efficiency in laser welding of highly reflective pure copper. J Mater Process Technol 216:287–293
11. Zhang YX, Gao XD, Katayama S (2015) Weld appearance prediction with BP neural network improved by genetic algorithm during disk laser welding. J Manuf Syst 34:53–59
12. Zhang MJ, Chen GY, Zhou Y, Liao SH (2014) Optimization of deep penetration laser welding of thick stainless steel with a 10 kW fiber laser. Mater Des 53:568–576
13. Zhang YX, Gao XD (2014) Analysis of characteristics of molten pool using cast shadow during high-power disk laser welding. Int J Adv Manuf Technol 70:1979–1988
14. Gao XD, Liu GQ (2015) Elucidation of metallic plume and spatter characteristics based on SVM during high-power disk laser welding. Plasma Sci Technol 17:32–36
15. Li SC, Chen GY, Zhou C (2015) Effects of welding parameters on weld geometry during high-power laser welding of thick plate. Int J Adv Manuf Technol 79:177–182
16. Zheng R, Zhang P, Duan AQ, Xiao P (2014) Measurement of laser welding pool geometry using a closed convex active contour model. Meas Sci Technol 25:365603-1-10
17. Quintino L, Liskevich O, Vilarinho L, Scotti A (2013) Heat input in full penetration welds in gas metal arc welding (GMAW). Int J Adv Manuf Technol 68:2833–2840
18. Luo M, Shin YC (2015) Vision-based weld pool boundary extraction and width measurement during keyhole fiber laser welding. Opt Lasers Eng 64:59–70
19. Gao XD, Chen ZQ (2015) Measurement of micro weld joint position based on magneto-optical imaging. Chin Phys B 24:018103-1-7
20. Huang Y, Xiao YL, Wang PJ, Li MZ (2013) A seam-tracking laser welding platform with 3D and 2D visual information fusion vision sensor system. Int J Adv Manuf Technol 67:415–426
21. Subudhi BN, Patwa I, Ghosh A, Cho SB (2015) Edge preserving region growing for aerial color image segmentation. Adv Intell Syst Comput 309:481–488
22. You DY, Gao XD, Katayama S (2015) Detection of imperfection formation in disk laser welding using multiple on-line measurements. J Mater Process Technol 219:209–220
23. Lin CH, Chen CC, Li HL, Liao JR (2014) Fast K-means algorithm based on a level histogram for image retrieval. Expert Syst Appl 41:3276–3283
24. Rajinikantha V, Couceirob MS (2015) RGB histogram based color image segmentation using firefly algorithm. Proc Comput Sci 46:1449–1457
25. Madhukumar S, Santhiyakumari N (2015) Evaluation of K-means and fuzzy C-means segmentation on MR images of brain. Egypt J Radiol Nucl Med 46:475–479